

# Intensity profiles of linearly polarized light backscattered from skin and tissue-like phantoms

## Alexander Sviridov

National Institutes of Health  
National Institute of Child Health and Human  
Development  
Bethesda, Maryland 20892-0924  
and  
Russian Academy of Sciences  
Institute for Laser and Information Technologies  
Troitsk, Moscow Region, 142190, Russia

## Victor Chernomordik Moinuddin Hassan

National Institutes of Health  
National Institute of Child Health and Human  
Development  
Bethesda, Maryland 20892-0924

## Angelo Russo

National Institutes of Health  
National Cancer Institute  
Radiation Biology Branch  
Bethesda, Maryland 20892

## Alec Eidsath<sup>†</sup>

National Institutes of Health  
Office of Research Services  
Division of Bioengineering and Physical Science  
Bethesda, Maryland 20892

## Paul Smith

National Institutes of Health  
Office of Research Services  
Division of Bioengineering and Physical Science  
Bethesda, Maryland 20892

## Amir H. Gandjbakhche

National Institutes of Health  
National Institute of Child Health and Human  
Development  
Bethesda, Maryland 20892-0924

## 1 Introduction

There is a significant interest in medicine and biology to define tissue layer thicknesses and to observe changes in tissue fiber orientation *in vivo*. Diseases such as graft versus host disease (GVHD) and systemic sclerosis and treatment procedures such as ionizing radiation for cancer treatment can initiate keloid formation and skin fibrosis, characterized histologically by a drastic modification of the collagen bundles. Fibrosis is caused by a change in the collagen or other fiber structure as a result of the skin being exposed to x-ray irradiation.<sup>1</sup> These structure modifications are related to the transition from normal to pathologic tissue. Different physical modalities based on absorption and/or scattering of electromagnetic, acoustic, or thermal waves have been used to ana-

**Abstract.** Anisotropy of mouse and human skin is investigated *in vivo* using polarized videoreflectometry. An incident beam (linearly polarized, wavelength 650 nm) is focused at the sample surface. Two types of tissuelike media are used as controls to verify the technique: isotropic delrin and highly anisotropic demineralized bone with *a priori* knowledge of preferential orientation of collagen fibers. Equi-intensity profiles of light, backscattered from the sample, are fitted with ellipses that appear to follow the orientation of the collagen fibers. The ratio of the ellipse semi-axes is well correlated with the ratio of reduced scattering coefficients obtained from radial intensity distributions. Variation of equi-intensity profiles with distance from the incident beam is analyzed for different initial polarization states of the light and the relative orientation of polarization filters for incident and backscattered light. For the anisotropic media (demineralized bone and human and mouse skin), a qualitative difference between intensity distributions for cross- and co-polarized orientations of the polarization analyzer is observed up to a distance of 1.5 to 2.5 mm from the entry point. The polarized videoreflectometry of the skin may be a useful tool to assess skin fibrosis resulting from radiation treatment. © 2005 Society of Photo-Optical Instrumentation Engineers. [DOI: 10.1117/1.1854677]

Keywords: light propagation in tissue; equi-intensity profiles of light; collagen fiber orientation; optical diagnosis; fibrosis.

Paper 04014 received Feb. 6, 2004; revised manuscript received May 28, 2004; accepted for publication Jun. 3, 2004; published online Feb. 10, 2005.

lyze tissue structure noninvasively.<sup>2-4</sup> The development of digital cameras has created new possibilities for video reflectometry,<sup>5</sup> polarimetry,<sup>6</sup> and polarized photography to map the structural characteristics of tissue.<sup>7,8</sup> Such cameras with increased dynamic range (12 bits and more) may be particularly useful in the measurement of 2-D intensity distributions, which result from a light beam being diffusively transmitted through or reflected from a turbid media.

The influence of relative orientations of collagen film samples and polarization analyzers on the angular distribution of linearly polarized light, transmitted through this film, has been analyzed previously.<sup>9</sup> In an earlier study,<sup>10</sup> it was shown both theoretically and experimentally that the anisotropy of scattered light is sensitive to fiber (rod) orientation, fiber thickness, and the spatial periodicity of the sample structure. Simple mathematical models of polarization rotation by rods

<sup>†</sup>A. Eidsath passed away before the paper submission. Address all correspondence to Victor V. Chernomordik, National Inst. of Health, Bldg. 12A, Rm. 2041, 9000 Rockville Pike, Bethesda, MD 20892-5626. Tel: 301-435-9236; Fax: 301-435-9236; E-mail: vchern@helix.nih.gov

were used to qualitatively describe observed intensity profiles.<sup>9,11</sup>

Recent studies have shown that observed deviations of the intensity distributions of scattered light from the circular symmetry can be related to the orientation of tissue fibers,<sup>12</sup> enabling the preferential orientation of tissue fibers to be determined. One may expect that these deviations from the symmetry of backscattering patterns can be related to the asymmetrical orientation of scattering elements of the media. In particular, collagen fibers and their bundles inside skin are believed to produce similar asymmetrical intensity profiles.

For example, ellipticities of spatially resolved intensity profiles, resulting from the forward scattering of light, have been correlated with fiber orientation of normal and scarred skin in histological samples.<sup>13</sup> The polarization structure of backscattered light reveals similar asymmetric features that result from the preferential orientation of tissue fibers. The issue of photon migration in anisotropic media has attracted special interest recently with regard to possible applications in brain imaging. Conventional diffusion approximation has been generalized for this case by Heino et al.<sup>14</sup> On the other hand, Dagdug et al.<sup>15</sup> modified the standard random walk theory for infinite semispace/slab geometries by using an anisotropic scattering coefficient with one of the major axes parallel to the surface. In this paper, the ellipticity of the equi-intensity profiles was predicted. It was characterized by an eccentricity factor proportional to the inverse ratio of the square roots of the scattering coefficients. This technique can also be effective when analyzing the distribution of light backscattered from media such as skin.

The purpose of this paper is to use the spatially resolved intensity profiles of different polarization states of incident and detected backscattered light to quantify the degree of structural anisotropy of the skin. The methodology used to assess the tissue anisotropy is based on pencil-beam illumination of the region of interest, combined with area detection. This illumination geometry provides several important advantages compared to a more commonly used scheme involving area illumination from an expanded laser beam, covering the whole image region (see e.g., Jacques et al.<sup>8</sup>). First, in the case of the focused incident light, the backscattered light may quantitatively probe the structure of deeper tissue layers because an effective penetration depth of the photons is determined by the separation between the photon entry point and detector (see e.g., Gandjbakhche and Weiss<sup>16</sup>). However, for the area illumination, the detected signal at each pixel is dominated by photons with entry points in the vicinity of each pixel, i.e., light, backscattered from the superficial layer of the sample. In addition, using a point light source can also reduce the pixel crosstalk, which is related to light scattering and has a detrimental effect on the image quality in the conventional scheme.<sup>8</sup> To avoid misunderstanding, note that the final goal is not to image the region of interest with the broad laser beam, as usually discussed in the literature. Instead, a methodology was developed to quantify the anisotropy of the sample from polarization measurements with pointlike illumination. Although, in fact, the model provides spatial “impulse” response function of tissues, at the current stage there are no plans to expand it to the area illumination setup because of the problems with the latter methodology already mentioned.

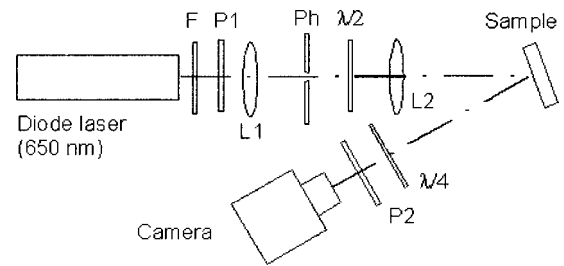


**Fig. 1** Schematic of the experimental setup: F, neutral filters; P1 and P2, polarizers; Ph, pinhole; L1 and L2, lenses;  $\lambda/2$ , half-wave plate; and  $\lambda/4$ , quarter-wave plate.

To substantiate the approach, two types of tissuelike phantoms with well-defined anisotropy properties were initially investigated. A delrin slab was used as a sample of optically isotropic media, while demineralized bone with known preferential orientation of collagen fibers was used as an example of optically anisotropic media. This preliminary study showed the ability of spatial intensity profile analysis to characterize the anisotropic optical properties of tissue, and consequently the extent of tissue fiber orientation. Finally, the anisotropy of mouse and human skin was investigated *in vivo* using the equi-intensity profile method.

## 2 Materials and Methods

The design of the experimental setup is shown in Fig. 1. A diode laser, emitting at a wavelength of 650 nm, was chosen to provide sufficient depth penetration of light into the sample. For all used tissuelike phantoms and skin, such light penetration (more than several mean scattering lengths, i.e., several millimeters) was achieved because their absorption at this wavelength is much smaller than the scattering.

The probe beam was directed in the horizontal plane and passed through the spatial filter consisting of two lenses (L1 and L2) and a pinhole (Ph) of 20  $\mu\text{m}$  diameter. The pinhole was imaged by L2 on the sample surface with a magnification of 1.5, giving a small 30- $\mu\text{m}$ -diameter spot. Neutral filters (F) of various optical densities were used to attenuate the laser light. One polarizer (P1) was used to provide the linear polarization of the probe beam. By rotating the half-wave plate ( $\lambda/2$ ), the orientation of the polarization of the incident beam was turned with respect to the axis of the probe beam.

To exclude specular reflection from the sample surface to sensitive elements of the camera, the surface of the sample was rotated around the vertical axis (tilt  $\sim 20$  deg relative to the direction of the probe beam), while the optical axis of the camera objective was oriented normally to the sample surface. This arrangement created, in principle, a slight asymmetry between the horizontal and vertical directions with respect to the probe beam and camera objective axis. However, for various polarization states of the probe beam, preliminary studies have shown no significant difference in asymmetry of diffusively backscattered light resulting from the sample tilt. The slight deviation from the circular symmetry of the intensity profiles for the isotropic delrin sample (eccentricity  $\sim 0.96$ ), observed far from the photon entry point (see Table 1) can be explained by the insufficient accuracy of our measurements of this parameter (m.s. error  $\sim 5$  to 8%). At the current stage, it is

**Table 1** Comparison of the ratio of semimajor axis lengths of equi-intensity ellipses in the far zone with the ratio of the square root of the slopes of appropriate dependence  $\ln[r^2 I(r)]$  as a function of  $r$ .

Sample	$(I_a/I_b)^{-2}$	$\mu'_{s,a}/\mu'_{s,b}$
Delrin	0.96	0.98
Demineralized bone	0.29	0.36
Human skin	0.64	0.67
Mouse skin	0.95	0.91

not possible to estimate the real tilt contribution to the profile asymmetry. The analyzer (P2) with a horizontally oriented transmission axis was located in front of the camera objective. The polarization vector of the incident beam was oriented either vertically to provide cross-polarized ( $H_v$ ) or horizontally for copolarized ( $H_h$ ) detection. A quarter-wave plate ( $\lambda/4$ ) was placed in front of the analyzer such that the reference axis was oriented horizontally, enabling transformation of the diagonal components of the linearly polarized scattered light into circular states that were nonspecific to the analyzer. This setup is known to be especially important when diagonally oriented four-leaf or fourfold cross-polarized patterns originate from a random distribution of surface and bulk non-homogeneities of the sample,<sup>17</sup> or even from a weakly scattered uniform medium.<sup>18</sup> The presence of the quarter-wave plate also enabled measurement of the Stokes parameters of backscattered light, when necessary.

To measure the intensity distributions, a digital camera [Canon, EOS D30, with maximum objective of 2.8 numerical aperture (NA) and a 0.31-m focal length] was used. Calibration of the camera response for focused and wide beams was performed using a set of neutral filters. The camera response proved to be practically linear over the broad range of intensities. This enabled regions of very low (those far from the focal point) or very high (those close to the focal point) intensities, where the SNR was not acceptable for precise measurement, to be excluded from the analysis by placing saturation restrictions on the matrix detectors. The equi-intensity profiles were mapped as a set of CCD matrix pixels corresponding to a chosen intensity level. Given that the distance between neighboring pixels in the CCD matrix corresponded to 0.02 mm on the sample surface, the pixel coordinates of the CCD matrix were transformed into real dimensions of intensity patterns. Thereafter, the experimental points were fitted with an ellipse (minimizing the deviation sums of squares from the ellipse and the experimental points). Two coordinates of the ellipse center, two semiaxis lengths and the azimuth angle between the horizontal axis in the laboratory coordinate system, and the closest axis of the ellipse were used as fitting parameters. The ellipse axis that least inclined to the horizontal axis in the laboratory Cartesian system is deemed the horizontal in the following text (angle  $\theta$  between these axes was in the range of  $-\pi/4 \leq \theta \leq \pi/4$ ). The experiments demonstrated that  $\theta$  was dependent on the length of the horizontal semiaxis of the ellipse (the intensity level).

Experiments were performed with samples of white Delrin resin, demineralized bone, mouse skin *in vivo*, and human

forearm skin *in vivo*. The Delrin sample was a disk of 10 mm thickness and 30 mm diameter. Delrin microstructure is known to be randomly oriented linear polymer molecules. Samples of demineralized bone were prepared from the tube bones of fresh chicken legs after a treatment with 0.5 M EDTA (pH 8.0) for 30 days at 4°C to remove the hydroxyapatite. The demineralized bone was 1.2 to 1.5 mm thick, had lateral dimensions of 15×25 mm, and consisted mainly of bone collagen having a preferential orientation along the longitudinal axis of the bone, as seen in the cross-polarized modes of the polarized microscopy.

Skin from the volar region of the forearm from normal human volunteers as well as skin from C3H/Hen mice was studied. The hairs on the mouse flanks were removed by plucking. Before the hair was removed and optical measurements were recorded, the mice were anaesthetized by an intraperitoneal injection of ketamine (100 mg/kg) and xylazine (10 mg/kg).

### 3 Results and Discussion

The raw data were analyzed and are being presented using several different methods. First, the variation of the equi-intensity profiles of the backscattered light was considered as a function of the distance from the photon injection point. In addition, the anisotropy of intensity-distance dependences was analyzed wherein the attenuation in the rates of backscattered light intensities along major axes were compared. Special attention was paid to the influence of the initial polarization state of light on the evolution of the equi-intensity profiles with the distance. The measurements showed qualitatively different behaviors for two limiting cases. The first was the near zone, corresponding to relatively small separations <1.5 to 2.5 mm between the entry and exit points of the photons, where photons underwent only a few scattering events in the medium before detection. The second was the far zone, corresponding to large distances of separation from the focal point (compared to scattering length) wherein almost all backscattered photons experienced multiple scattering events. For this reason, a diffusion-like model was used to describe photon migration in the far zone.

As expected, for the isotropic medium (delrin), the equi-intensity profiles of backscattered light were very close to circles for both analyzer-polarizer configurations and for the entire range of distances from the input point of the probe beam [Figs. 2(a) and 2(b)]. For the anisotropic medium (demineralized bone), the equi-intensity profiles had a pronounced oval shape well fit by ellipses [Figs. 3(a) and 3(b)]. These profiles depended strongly on the distance from the entry point and the state of polarization of the incident light. Figures 4(a) and 4(b) quantitatively illustrate the ratio of the ellipse semiaxes (eccentricity factor) as a function of the horizontal semiaxis length that corresponds to the profiles of Figs. 2 and 3. The eccentricity factor for delrin is close to one for the entire range of horizontal semiaxis lengths. For the demineralized bone, the shapes of the equi-intensity profiles proved to be quantitatively and qualitatively different in the near and far zones of the medium interface. In the near zone (<1.8 mm distance from the entry point), the backscattered light preserved memory about the polarization state of the probe beam that appeared, as a difference of eccentricity fac-

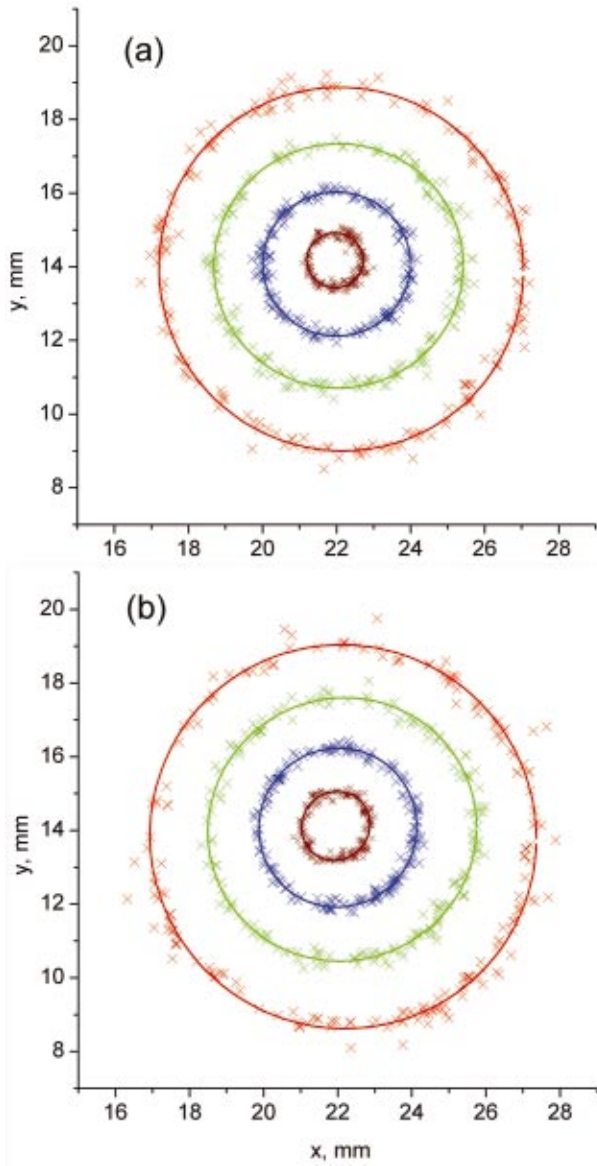


**Fig. 2** Equi-intensity profiles of pencil-like probe beam diffusively reflected from delrin slab and their elliptical fits for (a)  $H_v$  and (b)  $H_h$  configurations of analyzer-polarizer, respectively.

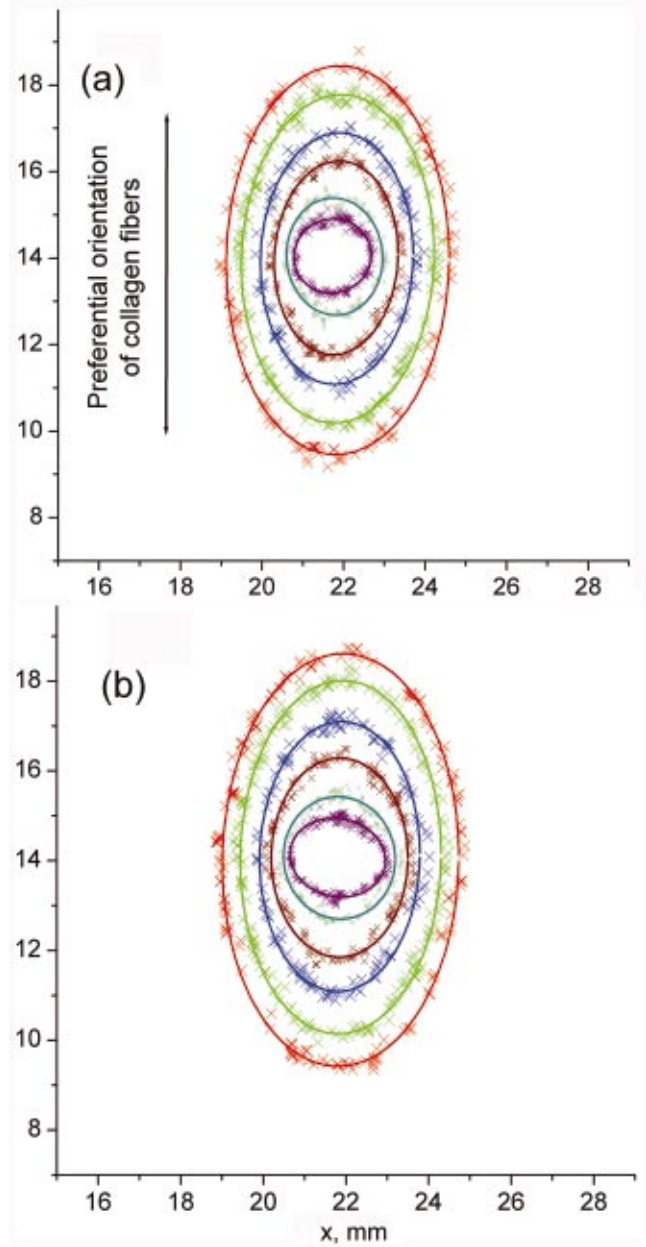


**Fig. 3** Equi-intensity profiles of the pencil-like probe beam diffusively reflected from the sample of demineralized bone and their elliptical fits. The collagen fibers of the sample were assembled vertically for (a)  $H_v$  and (b)  $H_h$  configurations of analyzer-polarizer, respectively.

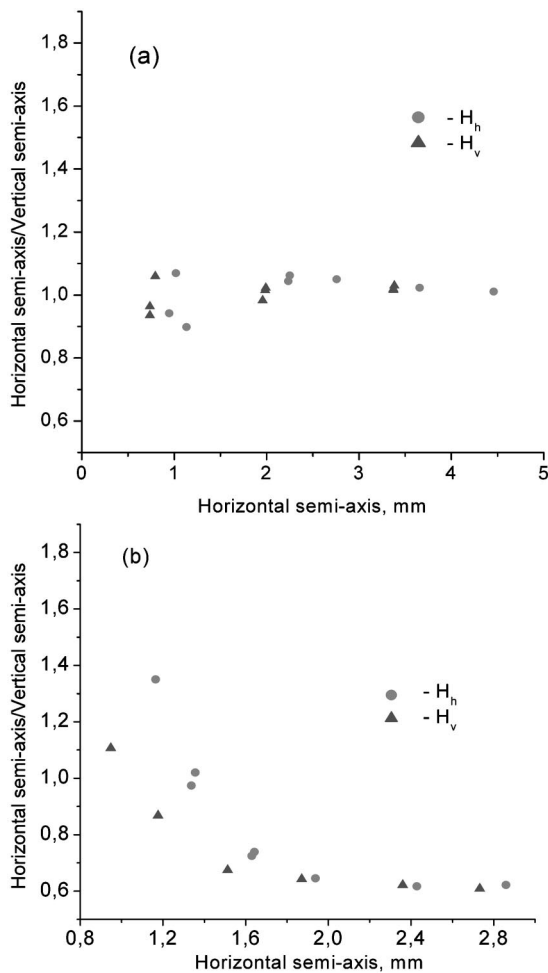


Fig. 4 Eccentricities of equi-intensity ellipses as a function of distance from the entry point for (a) delrin and (b) demineralized bone.

tors for  $H_v$  and  $H_h$  mutual orientation of analyzer and polarizer. In the far zone, the detected photons lost their initial polarization due to multiple scattering events. The shapes of the profiles (i.e., eccentricities) become independent of the initial conditions and distances traveled, but show sensitivity to the anisotropic structure of the medium.<sup>19</sup> Experimental data [Figs. 3(a) and 3(b)] obtained from samples with *a priori* knowledge of fiber direction, proved that equi-intensity ellipses in the far zone were elongated in the direction of the collagen fibers. On the contrary, in the near zone, the equi-intensity ellipses tended to be elongated perpendicular to the fibers, due to a higher scattering coefficient in this direction. Such behavior implies a 90-deg turn of the major axis of the equi-intensity ellipses, corresponding to a transition from small to large distances  $r$ . The magnitude of the observed eccentricities of these ellipses depends strongly on the distance  $r$  in the near zone. Kienle et al.<sup>10</sup> previously observed experimentally and modeled theoretically similar effects for anisotropic dentin.

The majority of the photons backscattered from the near zone underwent far fewer scattering events in comparison with the photons from the far zone. Consequently, they can be characterized by the different mean path and depth of the migration inside tissue. The relationship between an effective

penetration depth of the photons and source-detector separation were recently discussed.<sup>16</sup> The near-zone photons carry information mostly about the structure of a superficial layer of thickness of approximately one to two scattering lengths, while the data from the far zone provide important information about the anisotropy of the deeper layers of the medium.

The main features of the behavior of the intensity profiles for anisotropic media clearly appeared for human forearm skin [Figs. 5(a) and 5(b)]. A similar study with mouse skin [Figs. 6(a) and 6(b)] showed that its anisotropic factor is much less in comparison with human skin.

Both the model of light diffusion<sup>20</sup> and random walk theory<sup>21</sup> for semi-infinite turbid media predict the following asymptotic relationship between the logarithm of intensity  $I(r)$  measured with detectors of small aperture (pixel size) and scattering and absorption coefficients of the media:

$$\ln[r^2 I(r)] \propto (3\mu_a \mu'_s)^{-1/2} r, \quad (1)$$

where  $\mu'_s = \mu_s(1-g)$  is a transport-corrected scattering coefficient ( $g$  is the anisotropy factor),  $\mu_a$  is the absorption coefficient, and  $r$  is the distance between the entry point of the pencil-like probe beam and the exit (detection) point. Note that the expression  $(3\mu_a \mu'_s)^{-1/2}$  is defined as the attenuation coefficient  $\mu_{\text{eff}}$ . To avoid misunderstanding, noted that, while for the random walk model<sup>21</sup> unambiguously  $\mu_{\text{eff}} = (3\mu_a \mu'_s)^{-1/2}$ , there is some discrepancy in the literature about an exact expression for the attenuation coefficient  $\mu_{\text{eff}}$  in the diffusion model. This is related, in fact, to different definitions of the diffusion coefficient  $D$  used by different researchers. In the diffusion model  $\mu_{\text{eff}} = (\mu_a/D)^{1/2}$ , where  $D$  is determined either as  $D = [3(\mu'_s + \mu_a)]^{-1}$  (see, e.g., Patterson et al.<sup>22</sup> and Farrell et al.<sup>20</sup>) or  $D = (3\mu'_s)^{-1}$  (i.e.,  $D$  does not depend on the absorption coefficient).<sup>23-25</sup> Strictly speaking, the diffusion approximation is valid only if  $\mu_a \ll \mu'_s$ . For this reason, the difference between the two expressions for  $D$  should be negligible.

A larger  $\mu_{\text{eff}}$  results in a steeper rate of decrease of back-scattered light intensity with the distance  $r$ . Equation (1) was originally derived for the case of isotropic scattering structures. It results in circular equi-intensity profiles. In the case of anisotropic scattering structures with directionality parallel to the medium interface, the random walk model provides intensity-distance dependencies, qualitatively similar<sup>15</sup> to Eq. (1). However, the length  $l = (3\mu_a \mu'_s)^{-1/2}$ , characterizing the rate of intensity decrease with the distance in the diffusion mode, becomes dependent on the direction over the exit interface, in accordance with variation of the effective scattering coefficient along the major axes. Anisotropy of the absorption coefficient  $\mu_a$  is usually negligible when compared to the anisotropy of the scattering coefficient  $\mu'_s$ , which originates from the tissue structure. In this case, the lower probability of scattering in the direction parallel to the fiber axis than in the perpendicular direction<sup>26</sup> makes the equi-intensity profiles elliptical (with the major semiaxis parallel to the direction of the fibers) rather than circular.

At the same time, dependencies of  $\ln[r^2 I(r)]$  on distance  $r$  are expected to be linear in the diffusion mode of photon migration, for  $r > r_{\text{min}}$ . Here,  $r_{\text{min}}$  is a characteristic distance of transition from the near zone of photon migration (quasi-ballistic photons) to the far zone (photon diffusion). Slopes of

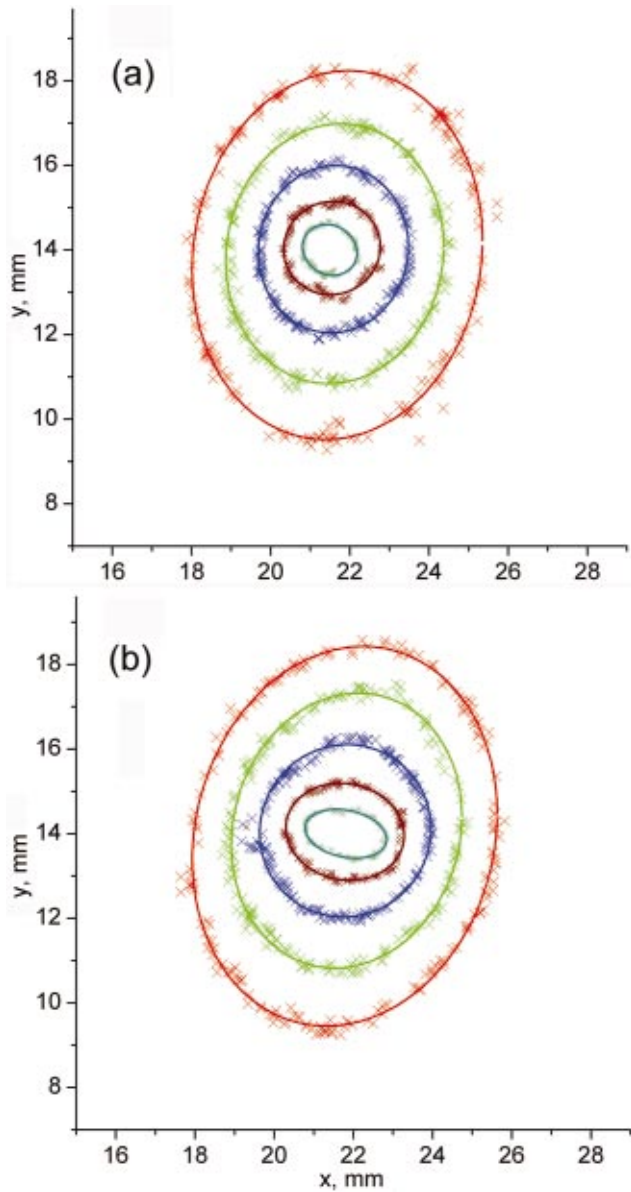


**Fig. 5** Typical equi-intensity profiles, originating from a pencil-like probe beam, diffusively reflected from human forearm skin *in vivo* and their elliptical fits for (a)  $H_v$  and (b)  $H_h$  configurations of analyzer-polarizer, respectively.

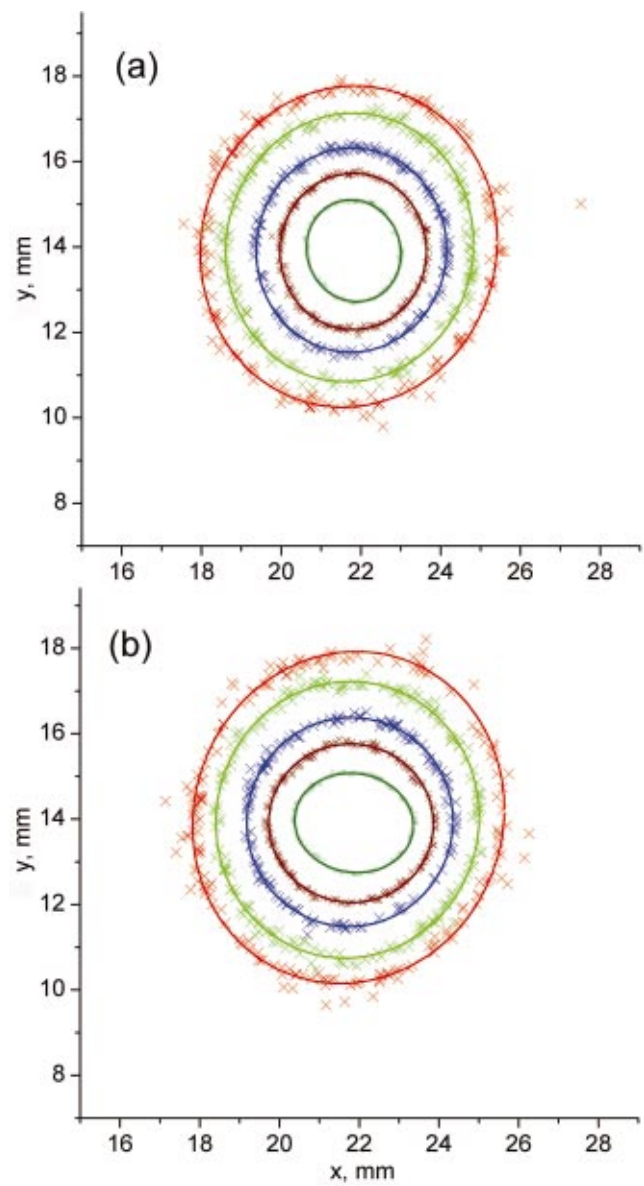


**Fig. 6** Typical equi-intensity profiles, originating from a pencil-like probe beam diffusively reflected from mouse flank skin *in vivo* and their elliptical fits for (a)  $H_v$  and (b)  $H_h$  configurations of analyzer-polarizer, respectively.

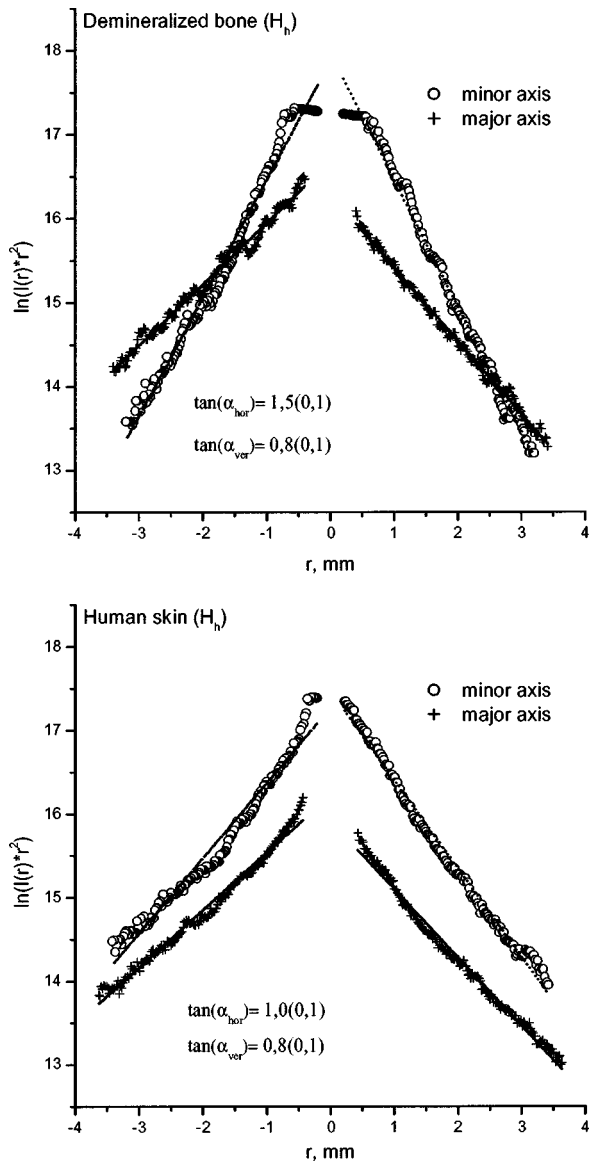


**Fig. 7** The dependence  $\ln[r^2 I(r)]$  for (a) demineralized bone and (b) human forearm skin, measured along the main axes of the external ellipse. Mean slopes of linear fits are shown for both vertical and horizontal axes.

these linear dependencies are proportional to the square root of the scattering coefficient in the given direction. Our experimental results clearly demonstrate a linearity of  $\ln[r^2 I(r)]$ , as a function of  $r$  in the broad range of distances,  $r > r_{\min}$ , where  $0.6 \text{ mm} < r_{\min} < 0.8 \text{ mm}$ . Corresponding data for demineralized bone and human forearm skin, measured in the  $H_h$  configuration, are plotted in Figs. 7(a) and 7(b) respectively.

Note that Bonner et al.<sup>27</sup> showed that the random walk formula used to derive the asymptotic Eq. (1) holds up for very small separations between the source and detector ( $r_{\min} \approx 0.6 \text{ mm}$ ) in the case of light backscattered from human skin.

Elongations of the equi-intensity profiles in the direction of collagen fibers for relatively large separations can also provide estimates of scattering anisotropy. Dagdug et al.<sup>15</sup> recently showed that in the diffusion mode of photon migration, the eccentricity of the equi-intensity ellipse was equal to

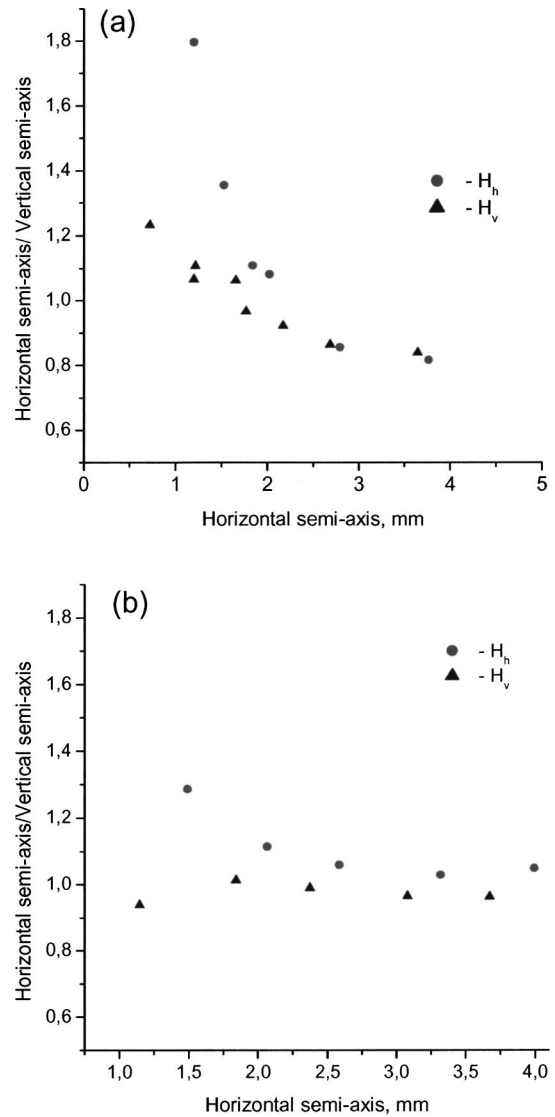


**Fig. 8** Eccentricities of equi-intensity ellipses as a function of distance from the entry point for (a) human skin and (b) mouse skin.

$(\mu'_{s,a}/\mu'_{s,b})^{1/2}$ , where  $\mu'_{s,a}$  and  $\mu'_{s,b}$  are reduced scattering coefficients along mutually perpendicular optical axes  $a$  and  $b$ , oriented parallel to sample surface. Intensities of the back-scattered light taken along the major axes of external equi-intensity ellipses are shown in Figs. 3 and 5. The ratio of the characteristic lengths, obtained from these intensity distributions, can be used to estimate the ratio of scattering coefficients in the directions parallel and perpendicular to the fibers.<sup>15</sup>

$$\mu'_{s,a}/\mu'_{s,b} = (l_a/l_b)^{-2}. \quad (2)$$

Table 1 shows the ratio of  $l_a/l_b$  obtained from equi-intensity ellipse measurements and  $\mu'_{s,a}/\mu'_{s,b}$  obtained as the square root of the slope of the function  $\ln[r^2 I(r)]$  on  $r$ . The results show agreement between the two methods used. Thus, from observed asymptotic values of these eccentricities [Figs. 4(b) and 8(a)] the following estimates of the scattering anisotropy were obtained. The values of  $\mu'_{s,a}/\mu'_{s,b}$  were approxi-

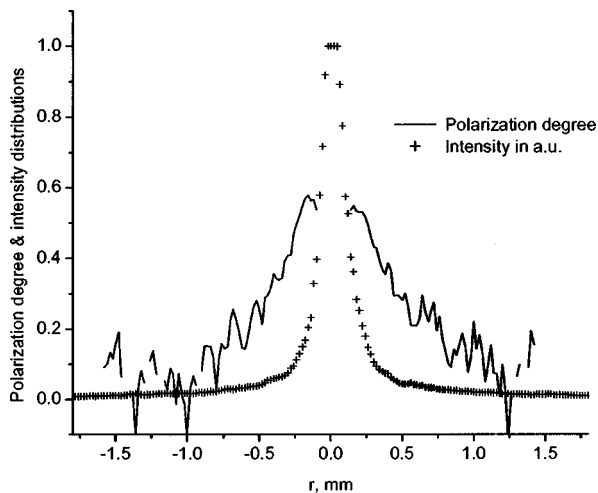


**Fig. 9** Depolarization of initially linearly polarized light with distance from the entry point (light is diffusively reflected by mouse skin).

mately 0.36 and 0.67 for demineralized bone and human skin, respectively. These values agree reasonably well (error < 20%) with the results found from axial intensity distributions. Note that the eccentricities method to estimate scattering anisotropy is likely to be more accurate because it is based on a self-consistent anisotropic model of the photon migration, while the method using analysis of the slopes of intensity distributions is just an extrapolation of the isotropic model of the photon migration. That is why the discrepancies between the results of two methods are expected to be maximal for media with the higher scattering anisotropy (i.e., demineralized bone).

Scattering anisotropy of the mouse skin proved to be considerably smaller ( $\mu'_{s,a}/\mu'_{s,b} \approx 0.91$ ) than for the human skin, likely because the mouse skin was less pronouncedly an anisotropic structure with shorter lengths of the corresponding fibers/bundles and/or lesser degree of their alignment. Also, normal human skin is much thicker than mouse skin and more highly structured initially as confirmed also by our measurements [Figs. 8(a) and 8(b)]. For the Delrin experiments, as expected, practically no anisotropy was observed.

Figures 4(b), 8(a), and 8(b) show these magnitudes for demineralized bone, human skin, and mouse skin, respectively. A strong dependence of the eccentricities on the relative configuration of the analyzer-polarizer pair is also observed at these distances. In particular, at small separations ( $r < 1$  mm) the eccentricities are much higher for the  $H_h$  configuration than for the  $H_v$  configuration. However, for the  $H_h$  configuration, they decrease much more rapidly with increasing  $r$ . At distances larger than some characteristic distance  $r_e$ , both geometries result in practically the same eccentricities. This finding means that the influence of the initial state of polarization of the incident light on equi-intensity profiles is preserved up to this distance. For analyzed samples of demineralized bone and skin,  $r_e$  varies between about 1.0 to 2.5 mm.

Depolarization of the backscattered light, estimated as the ratio of  $(I_{\text{par}} - I_{\text{per}})/(I_{\text{par}} + I_{\text{per}})$ , is illustrated in Fig. 9 as a function of the distance  $r$  from the beam entry point. Here, intensities  $I_{\text{par}}$  and  $I_{\text{per}}$  correspond to the  $H_h$  and  $H_v$  configura-

tions, respectively. For comparison, an intensity distribution is also presented in the same figure. Data points in the close vicinity of the entry point were excluded from the analysis of degree of polarization due to nonlinearity (saturation) of the light intensity measurements. At large distances from the entry point, the measured degree of polarization became too noisy and was also excluded from the analysis. Note that backscattered light intensity decreases much more rapidly with  $r$  than the degree of polarization. As seen in Fig. 9, the observed degree of polarization decreased from about 0.6 at a distance of  $\sim 0.2$  mm to the noise level at a distance of  $\sim 1.0$  mm. An alternative method of polarization estimates, based on the measurements of the Stokes parameters, was also applied (the data not presented here). No noticeable difference in the obtained degree of polarization was found when compared to results obtained from the previously described method. This is to be expected, if the circularly polarized component of the radiation is negligible. Under experimental conditions this component could possibly result from an initially linearly polarized light due to light scattering in the medium.

Assuming that the total number of scattering events does not depend on fiber orientation, then the polarization degree of any initially polarized beam decreases quickly with distance.<sup>28-30</sup> Note, however, that the relative orientation of the fibers and initial polarization vector of the incident light can contribute to the polarization degree of backscattered light. For example, it is well known that even initially nonpolarized light acquires some polarization due to scattering by the fibers when the polarization vector is parallel to the fibers axes.<sup>26,31</sup> Correspondingly, incident light, polarized along fiber assembly, is expected to preserve its polarization state over longer distances than light polarized perpendicularly to the fibers. The former polarization was actually realized in our experiments on demineralized bone, where the directionality of fibers was known *a priori*. The preservation of relatively large characteristic distances of polarization for bone and human skin (1.5 to 2.5 mm) seemed to exceed values expected just from the diffuse migration of photons. This may be explained either by the already mentioned additional polarization in the direction of fibers which originates from light scattering or possibly as a result of some waveguide effects<sup>32</sup> that can result in a fraction of photons to remain close to the surface due to multiple internal reflections, while migrating over long distances.

Note that subtracting the data obtained in the  $H_v$  configuration from the  $H_h$  data was suggested recently to adjust sensitivity of the imaging to different depths,<sup>6</sup> and in particular, to characterize skin pathologies by distinguishing superficially scattered light from diffuse light that has undergone many scatterings before detection.<sup>13</sup>

## 4 Conclusions

The equi-intensity profiles of pencil-like probe light diffusively reflected from skin and tissue-like phantoms are well fitted by ellipses. The orientation of the semimajor axis of the equi-intensity profile has a tendency to be perpendicular to the fiber orientation close to the entry point of the probe beam, while at larger distances the equi-intensity profile becomes parallel to

the fibers. The eccentricity of the equi-intensity profiles in the far zone increases with the fiber alignment degrees.

In the near zone (close to the entry point of the probe beam), the equi-intensity profiles depend on the mutual orientation of the sample, polarization vector of the incident beam, and the transmission axis of the analyzer relative to the direction of view. The eccentricity of the equi-intensity ellipses for copolarized and cross-polarized configurations depends on the extent of fiber alignment in the sample.

Monitoring the equi-intensity profiles of a pencil-like polarized beam, backscattered from the skin, can be a promising tool for characterizing fibrotic diseases that, in its turn, may provide a means for safer radiation treatment.

### Acknowledgments

A. Sviridov is thankful to the National Institutes of Health (NIH) for the support with a courtesy exchange grant and the Russian Foundation for Basic Research for partial support (grants NN 04-02-97203, 04-02-16743, and 04-02-16533).

### References

1. F. Berthod, L. Germain, H. Li, W. Xu, O. Damour, and F. A. Auger, "Collagen fibril network and elastic system remodeling in a reconstructed skin transplanted on nude mice," *Matrix Biol.* **20**, 463–473 (2001).
2. S. A. Telenkov, G. Vargas, J. S. Nelson, and T. E. Milner, "Coherent thermal wave imaging of subsurface chromophores in biological materials," *Phys. Med. Biol.* **47**, 657–671 (2002).
3. M. Fink, G. Montaldo, and M. Tanter, "Time-reversal acoustics in biomedical engineering," *Annu. Rev. Biomed. Eng.* **5**, 465–497 (2003).
4. X. C. Zhang, "Terahertz wave imaging: horizons and hurdles," *Phys. Med. Biol.* **47**, 3667–3677 (2002).
5. V. V. Tuchin, "Coherent optical techniques for the analysis of tissue structure and dynamics," *J. Biomed. Opt.* **4**, 106–124 (1999).
6. S. Y. Berezhna, I. V. Berezhnyy, and M. Takashi, "Dynamic photometric imaging polarizer-sample-analyzer polarimeter: instrument for mapping birefringence and optical rotation," *J. Opt. Soc. Am. A* **18**, 666–672 (2001).
7. S. L. Jacques, J. R. Roman, and K. Lee, "Imaging superficial tissues with polarized light," *Lasers Surg. Med.* **26**, 119–129 (2000).
8. S. L. Jacques, J. C. Ramella-Roman, and K. Lee, "Imaging skin pathology with polarized light," *J. Biomed. Opt.* **7**, 329–340 (2002).
9. M. Moritani, N. Hayashi, A. Utsuo, and H. Kawai, "Light-scattering patterns from collagen films in relation to the texture of a random assembly of anisotropic rods in three dimensions," *Polym. J. (Tokyo, Jpn.)* **2**, 74–87 (1971).
10. A. Kienle, F. K. Forster, R. Diebolder, and R. Hibst, "Light propagation in dentin: influence of microstructure on anisotropy," *Phys. Med. Biol.* **48**, N7–N14 (2003).
11. M. B. Rhodes and R. S. Stein, "Scattering of light from assemblies of oriented rods," *J. Polym. Sci.* **7**, 1539–1558 (1969).
12. S. Nickell, M. Heramnn, M. Essenpreis, T. J. Farrel, U. Kramer, and M. S. Patterson, "Anisotropy of light propagation in human skin," *Phys. Med. Biol.* **45**, 2873–2886 (2000).
13. A. G. Ferdman and I. V. Yannas, "Scattering of light from histologic sections: a new method for the analysis of connective tissue," *J. Invest. Dermatol.* **100**, 710–716 (1993).
14. J. Heino, S. Arridge, J. Sikora, and E. Somersalo, "Anisotropic effects in highly scattering media," *Phys. Rev. E* **68**, 031908 (2003).
15. L. Dagdug, G. H. Weiss, and A. H. Gandjbakhche, "Effects of anisotropic optical properties on photon migration in structured tissues," *Phys. Med. Biol.* **48**, 1361–1370 (2003).
16. A. H. Gandjbakhche and G. H. Weiss, "Descriptive parameter for photon trajectories in a turbid medium," *Phys. Rev. E* **61**, 6958–6962 (2000).
17. J. Borch, P. R. Sundararajan, and R. H. Marchessault, "Light scattering by cellulose. III. Morphology of Wood," *J. Polym. Sci.* **9**, 313–329 (1971).
18. M. Dogariu and T. Asakura, "Polarization-dependent backscattering patterns from weakly scattering media," *J. Opt. (Paris)* **24**, 271–278 (1993).
19. I. M. Stockford, S. P. Morgan, P. C. Chang, and J. G. Walker, "Analysis of the spatial distribution of polarized light backscattered from layered scattering media," *J. Biomed. Opt.* **7**, 313–320 (2002).
20. T. J. Farrell, M. S. Patterson, and B. Wilson, "A diffusion theory model of spatially resolved, steady-state diffuse reflectance for the noninvasive determination of tissue optical properties in vivo," *Med. Phys.* **19**, 879–888 (1992).
21. A. H. Gandjbakhche and G. H. Weiss, "Random walk and diffusion-like models of photon migration in turbid media," in *Progress in Optics*, E. Wolf, Ed., Vol. 34, pp. 333–402, Elsevier Science (1995).
22. M. S. Patterson, B. Chance, and B. C. Wilson, "Time resolved reflectance and transmittance for the noninvasive measurement of tissue optical-properties," *Appl. Opt.* **28**, 2331–2336 (1989).
23. M. Bassani, F. Martelli, G. Zaccanti, and D. Contini, "Independence of the diffusion coefficient from absorption: Experimental and numerical evidence," *Opt. Lett.* **22**, 853–855 (1997).
24. M. Morin, S. Verreault, A. Mailloux, J. Frechette, S. Chatigny, Y. Painchaud, and P. Beaudry, "Inclusion characterization in a scattering slab with time-resolved transmittance measurements: perturbation analysis," *Appl. Opt.* **39**, 2840–2852 (2000).
25. S. Carrarese, S. Tahani, F. Martelli, and G. Zaccanti, "Accuracy of a perturbation model to predict the effect of scattering and absorbing inhomogeneities on photon migration," *Appl. Opt.* **40**, 4622–4632 (2001).
26. C. F. Bohren and D. R. Huffman, *Absorption and Scattering of Light by Small Particles*, John Wiley & Sons, New York (1983).
27. R. F. Bonner, R. Nossal, S. Havlin, and G. H. Weiss, "Model for photon migration in turbid biological media," *J. Opt. Soc. Am. A* **4**, 423–432 (1987).
28. V. Sankaran, J. Walsh, T. Joseph, and D. J. Maitland, "Comparative study of polarized light propagation in biologic tissue," *J. Biomed. Opt.* **7**, 300–306 (2002).
29. D. A. Zimnyakov, Y. P. Sinichkin, P. V. Zakharov, and D. N. Agafonov, "Residual polarization of non-coherently backscattered linearly polarized light: the influence of the anisotropy parameter of the scattering medium," *Waves Random Media* **11**, 395–412 (2001).
30. F. C. MacKintosh, J. X. Zhu, D. J. Pine, and D. A. Weitz, "Polarization memory of multiply scattered light," *Phys. Rev. B* **40**, 9342–9345 (1989).
31. X. R. Huang and R. W. Knighton, "Diattenuation and polarization preservation of retinal nerve fiber layer reflectance," *Appl. Opt.* **42**, 5737–5743 (2003).
32. K. R. Forrester, R. Shymkiw, G. Yeung, P. Irwin, J. Tulip, and R. C. Bray, "Spatially resolved diffuse reflectance for the determination of tissue optical properties and metabolic state," in *Laser-Tissue Interaction XI: Photochemical, Photothermal, and Photomechanical*, D. D. Duncan, J. O. Hollinger, and S. L. Jacques, Eds., *Proc. SPIE* **3914**, 333–344 (2000).